Calibration and Validation of Direction-Finding High-Frequency Radar Ocean Surface Current Observations

Jeffrey D. Paduan, Kyung Cheol Kim, Michael S. Cook, and Francisco P. Chavez

***Abstract*—This paper focuses on the validation of remotely sensed ocean surface currents from SeaSonde-type high-frequency (HF) radar systems. Hourly observations during the period July 22, 2003 through September 9, 2003 are used from four separate radar sites deployed around the shores of Monterey Bay, CA. Calibration of direction-finding techniques is addressed through the comparisons of results obtained using measured and ideal (i.e., perfect) antenna patterns. Radial currents are compared with observations from a moored current meter and from 16 surface drifter trajectories. In addition, four overwater baselines are used for radar-to-radar comparisons. Use of measured antenna patterns improves system performance in almost all cases. Antenna-pattern measurements repeated one year later at three of the four radar locations exhibit only minor changes indicating that pattern distortions are stable. Calibrated results show root-mean-square (rms) radial velocity differences in the range of 9.8–13.0 cm/s, which suggest radar observation error levels in the range of 6.9–9.2 cm/s. In most cases, clear evidence of bearing errors can be seen, which range up to 30° for uncalibrated radar-derived radial currents and up to 15° for currents obtained using measured antenna patterns. Bearing errors are not, however, constant with angle. The results recommend use of measured antenna patterns in all SeaSonde-type applications. They also recommend an expanded simulation effort to better describe the effects of antenna-pattern distortions on bearing determination under a variety of ocean conditions.**

***Index Terms*—High-frequency (HF) radar, ocean currents, remote sensing.**

I. Introduction

SURFACE currents control transport and dispersion of buoyant particles in the coastal ocean. For this reason, knowledge of the velocity field is important to many ecological and societal problems. Knowledge of the two-dimensional (2-D) structure of the velocity field represents a challenging observational goal given the wide range of energetic processes. Some technologies, such as moored current meters, do a very good job resolving the temporal scales, but they fall short of monitoring, or even identifying, all of the relevant horizontal scales. Other technologies, such as arrays of accurately positioned drifting buoys, are capable of measuring the horizontal structure of the current field, but it is impossible to resolve the higher frequency processes for any particularly location over time.

The technology of radiowave backscatter measurements in the high-frequency (HF) portion of the electromagnetic spectrum provides a remote sensing technique capable of continuously monitoring surface ocean currents at time scales around 1 h. Furthermore, the commercially available systems have ranges of 50–200 km offshore and horizontal resolutions of 1–10 km. This combination makes HF radiowave (or HF radar) systems nearly ideal surface current mapping systems. The fact that the instrumentation is shore-based also makes it an ideal component of real-time and sustained environmental observing networks [1]. As a result of the combined scientific and monitoring benefits of HF radar, the number of individual systems deployed worldwide has increased dramatically in recent years. This expansion has also been due to increased networking capabilities and increased recognition of the need to monitor our coastal oceans.

The vast majority of HF radar instruments deployed for oceanographic purposes worldwide have been manufactured by one company, Codar Ocean Sensors, Ltd., Los Altos, CA.[1] The instruments have been variously called by the name coastal ocean dynamics applications radar (CODAR) or by the product name SeaSonde. Other types of HF radar systems have been produced, and others, such as the Wellen radar (WERA), are emerging as the applications grow [2]. Regardless of manufacturer, there is a universal need to characterize the accuracy of the radial current information produced by any given HF radar system. Basic validation studies have been conducted by a large number of research groups around the world. In most cases, the accuracy of HF radar-derived surface current observations has been bounded by making comparisons with vector velocity components from *in situ* current meters (e.g., [3]–[6]). Increasingly, this type of validation has been carried out more directly by comparing radial velocity components. That is, the *in situ* velocity component in the direction of the radar site is compared with the radial estimate from a single radar site (e.g., [7]–[9]). This is beneficial because errors related to the vector

Manuscript received November 28, 2004; accepted October 21, 2005. This work was supported by Center for Integrated Marine Technologies, National Oceanic and Atmospheric Administration (NOAA) under Grant NA160C2936, U.S. Office of Naval Research (ONR) under Grant N00014-02-0856, National Aeronautics and Space Administration (NASA) under Grant NAG5-12392, National Science Foundation (NSF) Global Ocean Ecosystems Dynamics (GLOBEC) under Grant 0000898, and David and Lucile Packard Foundation. **Associate Editor: L. R. Wyatt**.

J. D. Paduan and M. S. Cook are with the Naval Postgraduate School, Monterey, CA 93943 USA (e-mail: paduan@nps.edu; cook@nps.edu).

K. C. Kim was with the Naval Postgraduate School, Monterey, CA 93943 USA. He is now with the Republic of Korea Navy, Hyun-dong Chinhae City, Kyungsang Nam-Do 645-798, Republic of Korea (e-mail: sealion@hanafos.com).

F. P. Chavez is with the Monterey Bay Aquarium Research Institute (MBARI), Moss Landing, CA 95093 USA (e-mail: chfr@mbari.org).

Digital Object Identifier 10.1109/JOE.2006.886195

[1]http://www.codaros.com

mapping process, which uses data from two or more radars, are eliminated [10], [11].

Errors in HF radar-derived surface currents derive from a variety of sources, including radiowave interference, antenna distortions, unresolved velocity fluctuations, and insufficient degrees of freedom in the backscatter-to-radial current inversion algorithms. (Bearing angle errors related to antenna-pattern distortions are of particular interest to this paper and are described in more detail in the Appendix.) Comparisons with *in situ* data introduce additional velocity differences due to the mismatch in spatial and temporal averaging scales. The HF radar observations, for example, describe the velocity in the upper 1 m or so of the water column [12] averaged horizontally over 2–25 km^2 and in time over 0.3–1.0 h. None of the *in situ* observations match these parameters. In addition, the HF radar-derived estimates, which track the Doppler-shifted frequency of the Bragg-resonant surface gravity waves, are thought to include contributions from Stokes drift [13]–[15].

Calculations presented here were first described in [16]. In general, this investigation builds on the results of [7] who looked for evidence of bearing angle errors by comparing SeaSonde-derived radial currents with near-surface radial velocities from moored vector measuring current meter (VMCM) and acoustic Doppler current profiler (ADCP) observations. By using multiple *in situ* and HF radar locations, they were able to investigate 18 current-meter HF radar pairs in the Santa Barbara and Santa Maria Basins. They found bearing errors whose magnitudes ranged up to 19°. In the cases where more than one current meter was within the range of a single HF radar, the bearing errors were not constant as a function of angle, which rules out simple explanations related to incorrectly mounted receive antenna elements or current-meter compass offsets. In this paper, we repeat and extend the analyses of [7] using data from four SeaSonde HF radar systems mounted around the shore of Monterey Bay. Data from just one central ADCP mooring is available to compare with the HF radar data, but the shape of Monterey Bay provides the opportunity to investigate four radar-to-radar baseline comparisons in the manner of [17] and [18]. In addition, an array of surface drifting buoys was deployed as part of the U.S. Office of Naval Research's (ONR's) Autonomous Ocean Sampling Network (AOSN) program.[2] Those data span a wide range of angles relative to the four coastal radar locations making it possible to further describe bearing error as a function of angle.

Finally, this paper includes an assessment of the impact of using measured antenna patterns compared with the theoretical (or ideal) patterns within the multiple signal classification (MUSIC) direction-finding algorithm. *In situ* measurements of the antenna patterns were conducted at each of the radar sites during the period in question. Radial currents were computed using both ideal and measured patterns. Both sets of radial currents were compared to radial components from the ADCP and the drifting buoys, as well as to radial components from other radar sites that shared overwater baselines. As in [19], the use of measured antenna patterns improves the comparison between *in situ* and HF radar-derived radial velocity estimates. As in [19], we present evidence, from measurements separated by one year in time at a particular radar site, that antenna-pattern distortions are stable over time as long as physical conditions remain unchanged in the near-field of the receive antenna elements.

[2]http://www.mbari.org/aosn

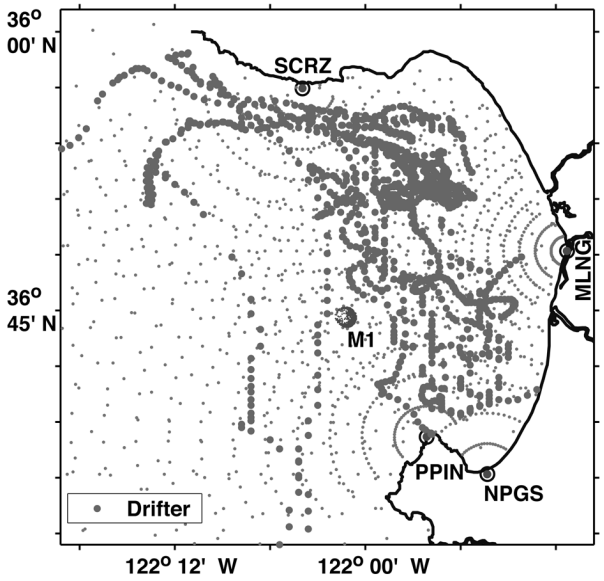

Fig. 1. Locations of four SeaSonde-type HF radar systems around Monterey Bay, CA, including Long Marine Laboratory in Santa Cruz (SCRZ), MBARI in Moss Landing (MLNG), the Naval Postgraduate School in Monterey Bay (NPGS), and the Point Pinos Coast Guard facility in Pacific Grove (PPIN). Nominal radial current observation positions are shown along arcs emanating from each radar site and the positions occupied by the mooring M1 within its watch circle are shown near the center of the Bay. Surface drifter positions (heavy symbols) from 16 independent deployments at the northern end of the Bay are also shown.

The organization of this paper is as follows. The data sources and their location and relative geometry are described in Section II along with the observed antenna patterns at each of the four HF radar sites. In Section III, radial current comparison statistics are presented for HF radar-to-ADCP, HF radar-to-HF radar (baseline), and HF radar-to-drifter, respectively. In Section IV, the results are discussed with regard to the observed uncertainties in HF radar-derived radial currents, the improvements obtained using measured antenna patterns over ideal antenna patterns, and the continuing need to extend this type of work using numerical simulations in which the true limitations of the MUSIC direction-finding algorithm can be explored under a variety of oceanographic conditions and antenna-pattern distortion scenarios.

II. Data Sources and Antenna-Pattern Measurements

The data described here were collected in the region of Monterey Bay, CA, during the period of the AOSN-II experiment in August and September 2003. Locations of four SeaSonde-type HF radar sites, one deep-ocean mooring and 16 satellite-tracked surface drifting buoy trajectories are shown in Fig. 1. The nominal radial current observation locations for each HF radar site and the observed watch circle of the M1 mooring maintained by the Monterey Bay Aquarium Research Institute (MBARI) are shown as light symbols on the figure. The offshore range resolutions of the radar systems were set to 3 km in the case of

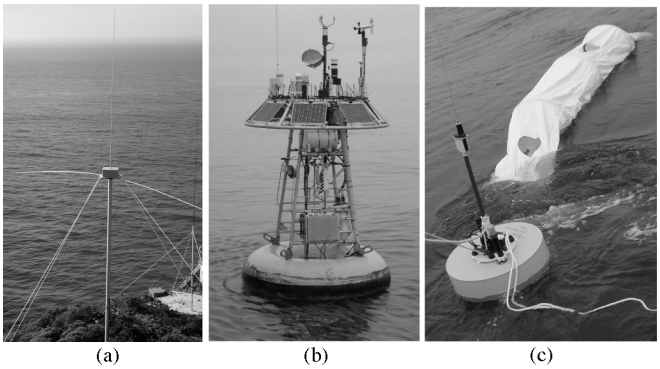

Fig. 2. (a) Example SeaSonde receive antenna with transmit antenna in the background. (b) Surface float and instrumentation on the MBARI M1 mooring. (c) MBARI instrumented drifter with its 5-m-long drogue element shortly after deployment.

the Santa Cruz, Naval Postgraduate School, and Point Pinos installations, which operated using radiowave frequencies around 13 MHz. The range resolution of the Moss Landing site, which operated using a frequency around 25 MHz, was 1.5 km. The watch circle of the M1 mooring, which was deployed in water depths around 1000 m, had a diameter of 2 km with the majority of locations clustered in the east and southeast directions consistent with forcing by the predominately northwesterly winds.

As mentioned previously, HF radar-derived radial velocity estimates respond to currents in the upper 1 m of the water column and are averaged over 1 h and several square kilometers. By contrast, the ADCP on the M1 mooring was a downward-looking unit mounted in a cage below the surface float [20]. During this period, the shallowest bin averaged the currents between 12 and 20 m. Similarly, the surface drifter positions responded to flow against the 5-m-long holey sock drogue element, which was centered around 5.5-m depth (Fig. 2). The mismatch in averaging scales and depths between the HF radar-derived radial currents and the ADCP- or drifter-based measurements accounts for a portion of the observed velocity differences. They do not, however, account for the observed bearing errors or variation in bearing errors or the observed improvement when measured antenna patterns are used in the direction-finding algorithm, which are the critical points of this paper.

A. Surface Current and Wind Patterns Around Monterey Bay

The study area in Monterey Bay is part of the California Current System along the United States west coast about 100 km south of San Francisco Bay. The oceanographic conditions in terms of surface currents are dominated by the cycle of upwelling-favorable winds from the northwest interrupted by shorter periods of weak or reversed wind forcing [21]. These conditions produce strong variations in surface currents in both space and time, which provide a range of radial current observations from which to test the performance of the four HF radar sites stations around the shoreline.

A synopsis of the oceanographic conditions encountered during this experiment is presented in Fig. 3, which shows the winds and 16-m current observations from the M1 mooring. The figure also shows representative surface current maps from

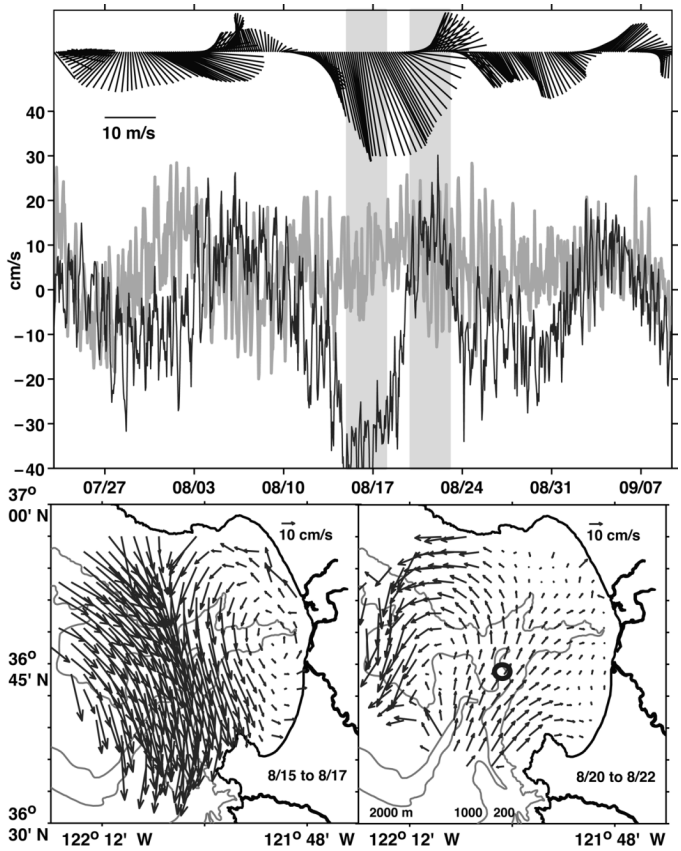

Fig. 3. Wind vectors, east–west current (light), and north–south current at the M1 mooring (upper) and HF radar-derived surface currents during upwelling- (lower left) and downwelling-favorable (lower right) wind conditions. The approximate mooring location (circle) is shown in the lower right panel and the averaging times (shaded boxes) are denoted in the upper panel.

the HF radar network. In this case, the maps show three-day averages of surface currents during contrasting upwelling- and downwelling-favorable wind conditions. The former conditions dominate the spring and summer seasons in the region creating a strong alongshore flow across the mouth of Monterey Bay with a cyclonic circulation cell within Monterey Bay [4]. The "relaxation" or downwelling-favorable conditions produce a narrow poleward flow reversal across the mouth of Monterey Bay that passes by the location of the M1 mooring. In addition to the subtidal-period variations, the moored current observations show higher frequency fluctuations related to semidiurnal tidal currents and diurnal sea breeze-driven currents. These fluctuations, although not shown here, are also present in the hourly HF radar-derived currents as reported in [4], [22], and [23].

B. Antenna-Pattern Measurements

The SeaSonde systems utilize a crossed-loop/monopole receive antenna configuration (Appendix). The design is particularly convenient because of its compact size. Two orthogonally mounted loops are housed inside a small receive box about 25 cm on a side and a single monopole whip runs through the middle (Fig. 2). In a distortion-free environment, the response patterns of the loop antenna elements are cosine functions of

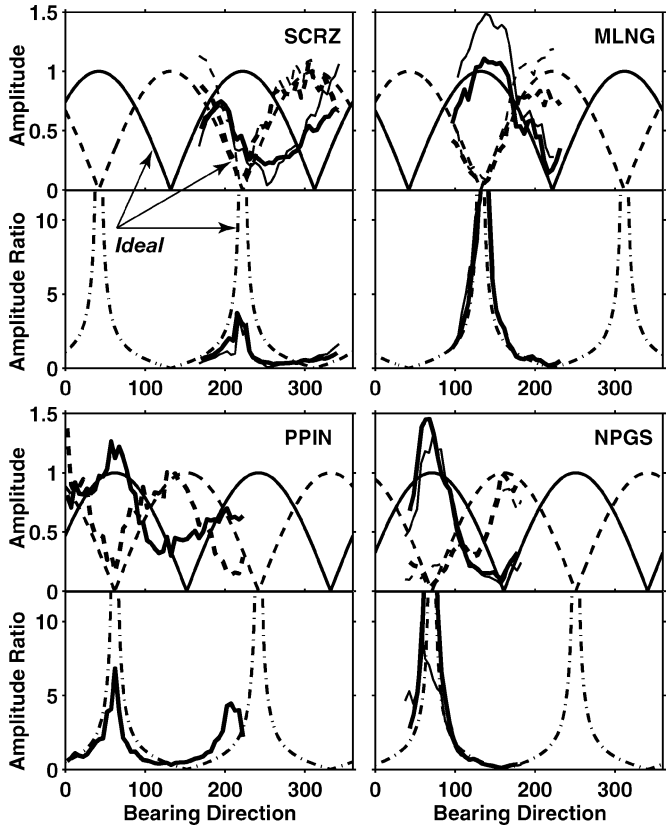

Fig. 4. Antenna element response patterns as a function of angle for loop 1 (solid) and loop 2 (dashed) as measured in August and September 2003 and as predicted based on ideal patterns, along with the ratio of loop 1 to loop 2 for the measured (solid) and ideal (dash–dot) patterns. Repeated measurements one year later at all but the PPIN location are also shown (thin lines).

angle when normalized by the monopole signal. These ideal patterns and the ratio between them are shown in Fig. 4 along with the measured antenna patterns at each of the four HF radar sites.

Collection of measured antenna-pattern data is relatively straightforward. In the case of the commercial SeaSonde instruments, a transponder unit is available that echoes the transmitted signals from the radar unit. Calibration data is collected by moving the transponder in a slow arc about 1 km offshore using a small boat or personnel watercraft and simultaneously recording global positioning system (GPS) positions. The transponder echo includes a user-selectable time delay that places the transponder peak in a measurement range cell that lies outside the near-shore blanking region. SeaSonde calibration software is also available that records the strength of the transponder echo and later merges that data with the GPS positions. In this way, the amplitudes and phases of the antenna response on each of the three elements can be determined as a function of angle. The angular resolution of the data is typically about 1°, which is higher than the 5° resolution of the direction-finding algorithm. By repeating the measurement arc in the opposite direction, it is also possible to verify the accuracy of the angular response pattern. Calibration data for other types of HF radar systems can be collected using a similar procedure, although it may be necessary to use a modified transmit unit in lieu of a transponder.

The severity and character of the antenna-pattern distortions are different at each of the four sites. Comparing the ideal and measured patterns in Fig. 4 suggests that they could be expected to produce different results. However, the exact effects of pattern distortions are not easily predicted. All direction-finding algorithms depend on clear distinctions between the maxima and minima of the ratio functions. Hence, it could be predicted that distortions that alter the alignment between maxima and minima, or distortions that produce additional local maxima and minima, will lead to the largest pointing errors. With this in mind, the SCRZ and PPIN sites appear to have the most significant pattern distortions, while the MLNG site appears to have the least amount of distortion. Pattern measurements were repeated at three of the four sites one year later in October 2004. With respect to the number and alignment of maxima and minima, the antenna patterns appear to have been quite stable from one year to the next. Amplitude variations were observed, however, particularly at the MLNG site. As mentioned previously, the significance of such changes is not clear. Likely, additional simulation work using the MUSIC algorithm under controlled conditions will be needed to quantitatively assess these effects.

III. Radial Current Comparison Statistics

A. Moored Velocity Comparisons

Comparison of HF radar-derived velocities with moored *in situ* observations is the method most commonly used to validate the remotely sensed surface currents. That exercise is repeated here using the M1 ADCP observations during the period from July 22, 2003 through September 9, 2003. The hourly vector velocity time series from M1 was corrected for mooring motion using GPS position data and then projected onto the directions of the four different HF radar sites according to $S_{\mathrm{M1}} = u_{\mathrm{M1}} \cos\alpha + v_{\mathrm{M1}} \sin\alpha$, where S_{M1} is the radial velocity in the direction of the radar site, α is the angle between M1 and the radar site, and u_{M1} and v_{M1} are the east and north velocity components at the M1 location, respectively.

The nature of HF radar estimates using direction-finding algorithms is such that one Doppler backscatter spectrum is obtained for each range. Each Doppler bin within the broadened Bragg-resonant spectral peaks determines a radial velocity approaching or receding from the radar site. The direction-finding algorithm must assign that speed to one or more angles, depending on the spatial complexity of the ocean current pattern. The number of angles that can be assigned to a given radial velocity observation is a function of the number of colocated antenna elements and the particular algorithm being used (Appendix; [24]). Because of this, radial current observations at a given range are not independent and pointing errors are manifest by placing a correct radial current at the wrong angular position. To test for this possibility, we compared the radial current time series observed at M1 with the radial current time series produced by the various HF radar instruments at multiple locations at the same range. This was done in addition to the detailed assessment of the observation bin closest to the mooring location. The geometry of these comparisons is

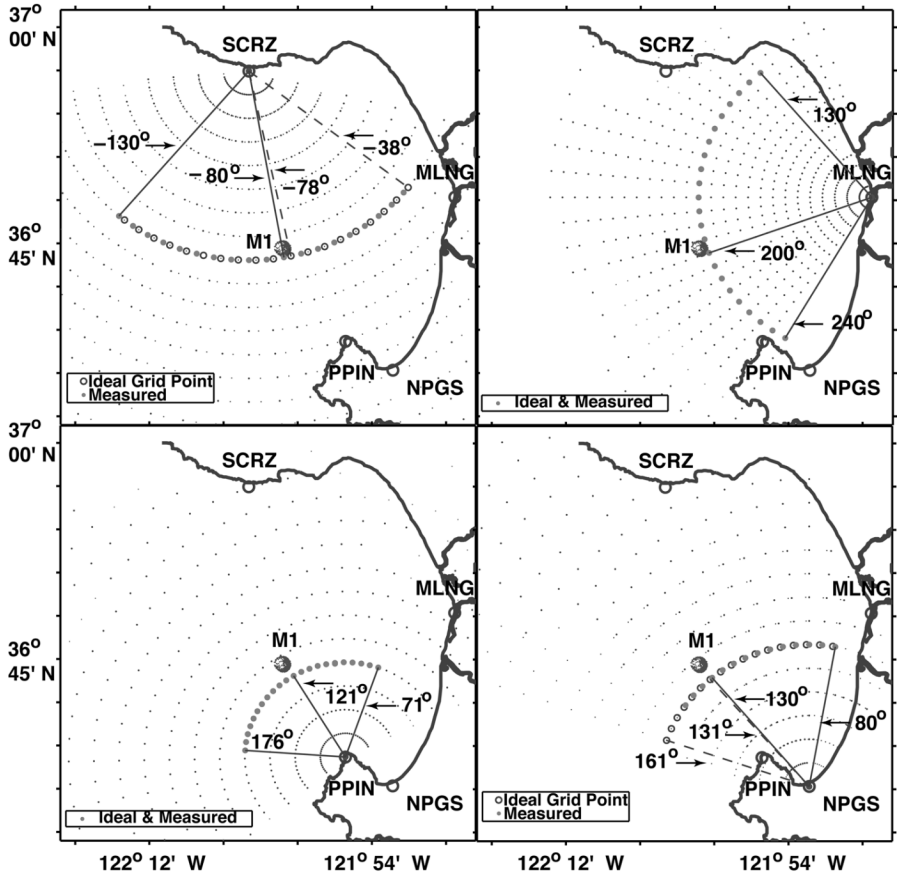

Fig. 5. Radial current observation grid locations for each HF radar site along with the constant-range locations closest to the mean location of the M1 mooring. Radial grid locations for SCRZ and NPGS sites are offset slightly for the ideal and measured antenna-pattern results. Angle values are measured counterclockwise from east and they denote the M1 direction as well as the limiting directions for which radial velocity comparisons were conducted at each site.

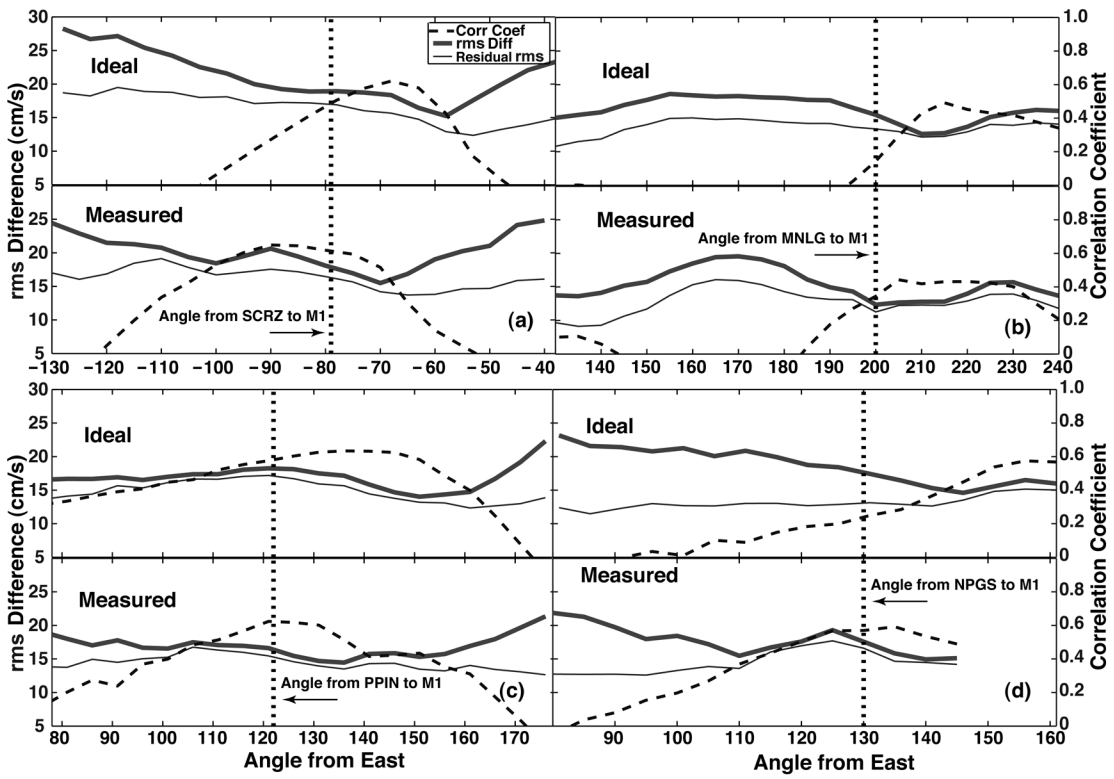

Fig. 6. Correlation, rms difference, and residual rms difference between radial currents at M1 and (a) SCRZ, (b) MLNG, (c) PPIN, and (d) NPGS HF radar sites for radar-derived currents using ideal and measured antenna patterns.

TABLE I
RADIAL CURRENT COMPARISON STATISTICS FOR GEOGRAPHICALLY MATCHED LOCATIONS

SCRZ versus:	**Correlation Coefficient**	**rms Diff (cm/s)**	**Res rms (cm/s)**	**Δθ* (°)**	**N**
M1-Ideal	*0.50*	*18.9*	*16.9*	*30*	*1073*
M1-Measured	0.62	18.1	16.5	10	942
MLNG-Ideal	*0.63*	*11.2*	*10.8*		*718*
MLNG-Measured	0.60	12.9	11.6	10	720
NPGS-Ideal	*0.44*	*28.5*	*11.2*		*409*
NPGS-Measured	0.79	11.8	11.4	–5	778
PPIN-Ideal	*0.66*	*17.3*	*14.1*		*696*
PPIN-Measured	0.81	13.0	10.5	0	760
Drifter-Ideal	*0.65*	*16.9*	*18.7*		*931*
Drifter-Measured	0.74	12.7	13.1		931
MLNG versus:	**Correlation Coefficient**	**rms Diff (cm/s)**	**Res rms (cm/s)**	**Δθ* (°)**	**N**
M1-Ideal	*0.14*	*15.5*	*13.4*	*10*	*1041*
M1-Measured	0.34	12.4	11.3	0	973
PPIN-Ideal	*0.57*	*13.3*	*10.8*		*503*
PPIN-Measured	0.66	9.8	8.5	0	790
Drifter-Ideal	*0.74*	*9.7*	*9.3*		*987*
Drifter-Measured	0.72	10.0	9.6		987
NPGS versus:	**Correlation Coefficient**	**rms Diff (cm/s)**	**Res rms (cm/s)**	**Δθ* (°)**	**N**
M1-Ideal	*0.25*	*17.4*	*13.1*	*15*	*637*
M1-Measured	0.57	17.6	16.6	10	822
Drifter-Ideal	*0.48*	*17.4*	*20.3*		*547*
Drifter-Measured	0.79	10.4	11.0		547
PPIN versus:	**Correlation Coefficient**	**rms Diff (cm/s)**	**Res rms (cm/s)**	**Δθ* (°)**	**N**
M1-Ideal	*0.58*	*18.3*	*17.2*	*30*	*884*
M1-Measured	0.62	16.6	15.5	15	1076
Drifter-Ideal	*0.74*	*11.8*	*12.0*		*610*
Drifter-Measured	0.77	10.4	9.7		610

*Based on angular location of minimum RMS difference.

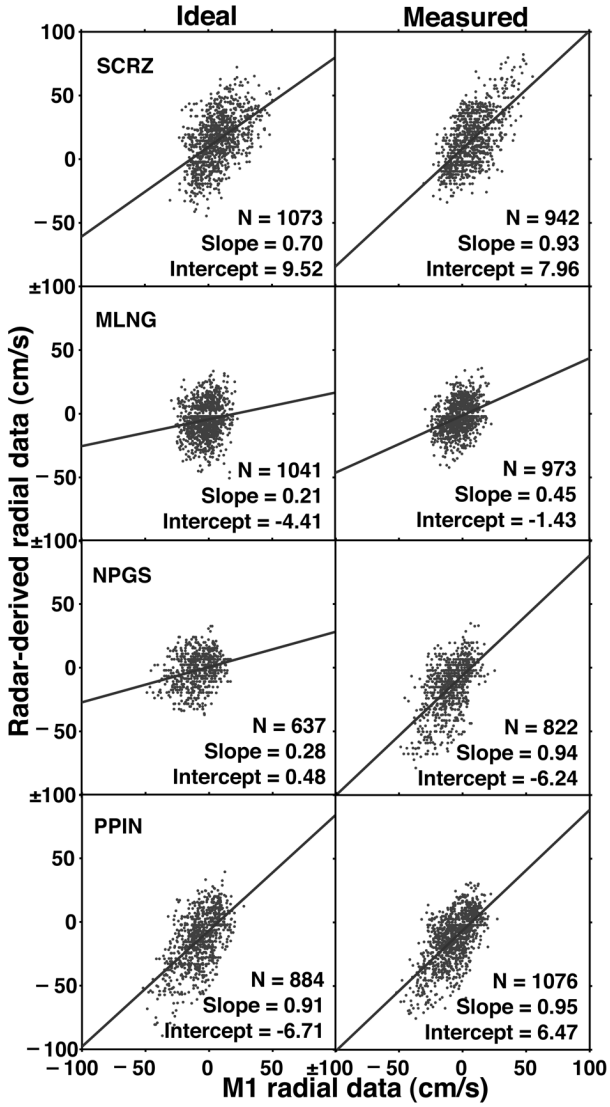

Fig. 7. HF radar-derived radial currents at the location of the M1 mooring against observations projected into the directions of the four radar sites. The number of hourly observations (N) and the slope and intercept for the best-fit linear prediction are also shown.

illustrated in Fig. 5, which shows the M1 mooring watch circle in relation to the closest range arc for each of the HF radar sites. (Note: The SCRZ and NPGS sites have slightly offset radial current observation grids due to the bounding angles contained in the measured antenna patterns at those sites. These 1° or 2° differences represent small offsets in the centers of the 5°-wide measurement cells. Also, the next furthest range arcs for the PPIN and NPGS radar sites appear to be closer to the M1 mooring. However, the selected range arcs are closer to the weighted average position of the M1 mooring, which is along the southeastern portion of the watch circle.)

Comparisons of radial currents observed at M1 and those estimated from the four HF radar sites are shown in Fig. 6. Each of the statistical comparisons is repeated using estimates based on both ideal and measured antenna patterns. The statistics include the magnitudes of the correlations, the root-mean-square (rms) differences, and the residual rms differences. In the latter case, differences were computed after removing the best-fit linear prediction of the radar-derived radial current as a function of the observed radial current at M1. This procedure allows for the physically realistic scenario that the ∼1-m-deep HF radar-derived velocity estimates have larger magnitudes than the velocities measured several meters below. The residual rms difference values should, therefore, be less than or equal to the basic rms differences.

Several conclusions can be drawn from the results in Fig. 6. First, it should be noted that the expected angular positions of the maximum correlation values and the minimum rms difference values are denoted by the vertical dashed lines on each of the panels. Those are the angles geometrically closest to the mean position of the M1 mooring. At each of the radar sites, there is evidence for some angular offset between the expected "best-match" angle and the angles observed to produce the highest correlation and/or lowest rms differences. For the most part, the angular location indicated by the maximum correlation value is the same as the one indicated by the minimum rms difference values. However, in some cases the two angle estimates diverge. In the case of the measured pattern results for SCRZ, the maximum correlation angle predicts an offset of 10° in the clockwise direction while the minimum rms differences predict an offset of 10° in the counterclockwise direction. The observed correlation, rms difference, and angular offset values for the expected best-match location are shown in Table I.

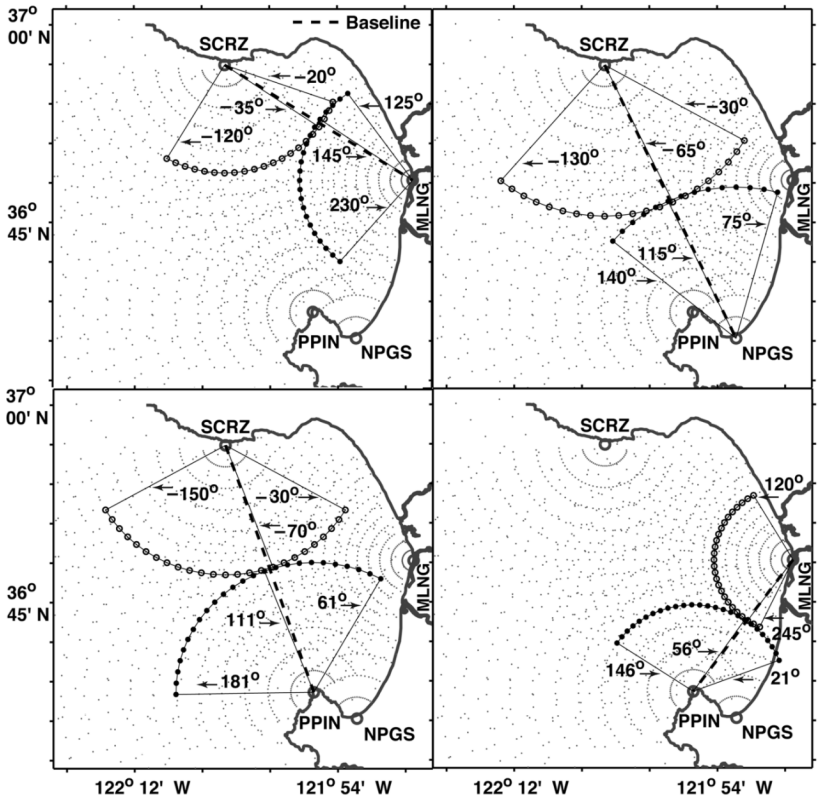

Fig. 8. Radial current observation grid locations and the baselines between pairs of HF radar sites along with the constant-range locations closest to the center point of the baselines. Angle values are measured counterclockwise from east and they denote the look direction between radar sites and the angular limit of the constant-range comparisons.

It is important to note that the statistical values in Fig. 6 are improved, in terms of magnitude and angular location, when results using measured antenna patterns are compared with those obtained using ideal antenna patterns. The most significant improvements are seen for the NPGS radar site, for which the results obtained assuming ideal antenna patterns are particularly poor. Apparently, the use of the measured patterns in the MUSIC direction-finding algorithm is able to correct for some pointing errors related to distortions of the receive antenna elements.

The scatter plots of radar-derived and observed radial currents at the expected best-match angles are shown in Fig. 7 for data obtained using both ideal and measured antenna patterns. The best-fit linear prediction parameters are also shown on the figure for each case (the correlation and rms difference values are summarized in Table I). In this presentation, the dramatic improvement obtained at the NPGS site using measured antenna patterns is clear. The improvement is more subtle at the other radar locations. It is also clear that the correlation values, in particular, are low for the MLNG location because the range of observed radial velocity values is relatively low. Curiously, the best-fit linear prediction lines do not reflect the visual impression given by the scatter plots nor do they reflect the expectation that radar-derived velocities at 1-m depth will be stronger than those measured by the ADCP at 16-m depth, which predicts a best-fit slope greater than 1. The least-square fit parameters are dominated by the large number of observations with small magnitudes, many of which cannot be identified in the figure because they are overplotted at the same location as another data point. In addition, the HF radar velocity resolution of about 2.5 cm/s may have skewed the slope estimates toward smaller values, although this is speculative.

B. Baseline Velocity Comparisons

The Monterey Bay geometry, coupled with the large number of HF radar sites in the region, provides for an opportunity to investigate four separate overwater baselines. This is particularly useful in terms of identifying the intrinsic level of velocity uncertainty in the HF radar estimates because all the time and space scales in the measurement can be exactly matched. Reference [18] illustrates the potentially large effect of disparate horizontal averaging scales when radial values are compared close to one radar site but far away from the second radar site. In this paper, we restrict the comparisons to the center location along the various baselines. In an error-free network, the radial velocity estimates at the center of the overwater baseline between two HF radar sites would be identical, apart from the factor of -1 needed to account for the opposite perspectives of approaching and receding Bragg waves.

The geometries of the four baseline comparisons are illustrated in Fig. 8. To look for further evidence of bearing errors, the comparisons were made from the perspective of each radar site. The radial time series along the expected baseline direction for one site was held fixed and compared with multiple radial time series at the same range and for multiple angles from the

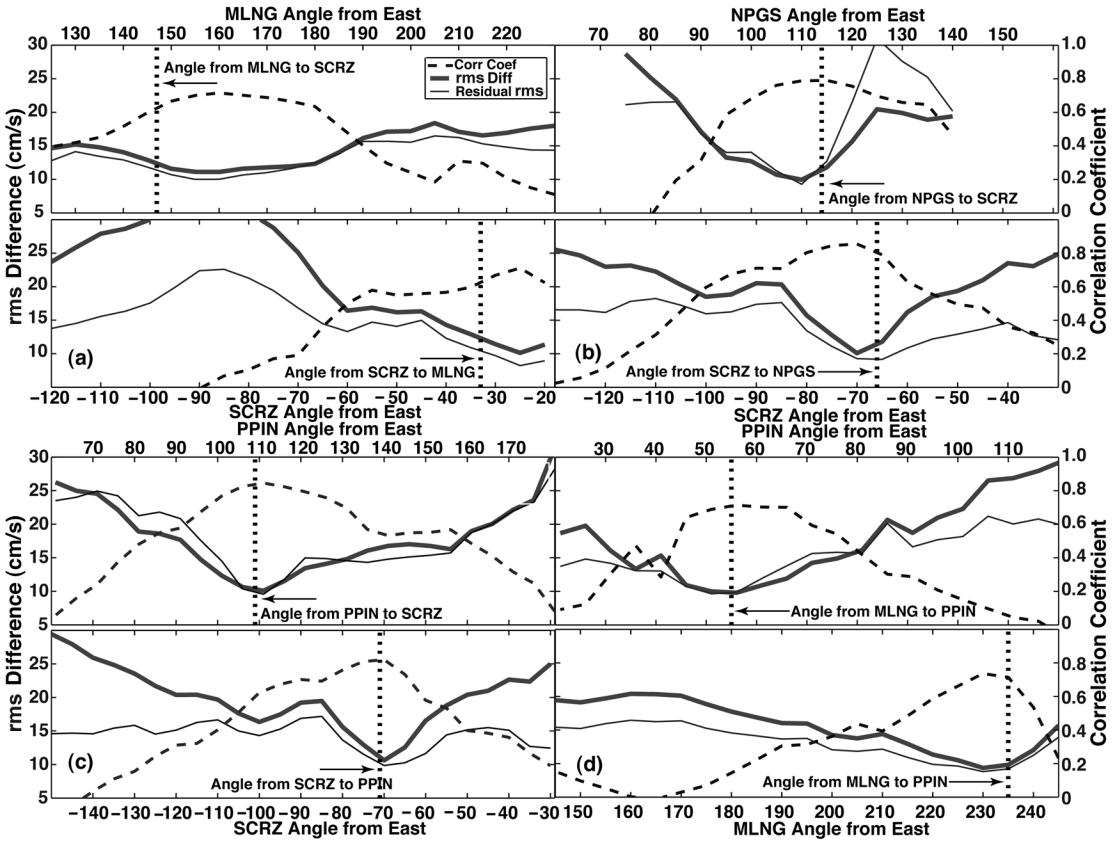

Fig. 9. Correlation, rms difference, and residual rms difference for radial currents estimates obtained using measured antenna patterns for baseline site pairs (a) SCRZ-MLNG, (b) SCRZ-NPGS, (c) SCRZ-PPIN, and (d) PPIN-MNLG.

opposite radar site. Then, the process was reversed and the radial time series along the expected baseline direction from the opposite radar site was compared with multiple radial time series at the same range from the original radar site.

Results of the statistical baseline comparisons are shown in Fig. 9 for various angles. As was the case for the fixed-point mooring comparisons, the correlation magnitudes and rms differences vary with angle and, in most cases, do not exhibit extrema at the expected bearing locations. Bearing errors of 5°–10° are common, although the error for the PPIN-to-SCRZ baseline is smaller than the 5° resolution of the measurements. The PPIN-to-SCRZ results, in particular, exhibit the type of angular response that provides a clear indication of how well the instruments were able to point along the baseline direction. The correlation and rms difference functions are highly peaked. The correlation is maximum in the baseline direction and it drops off quickly when data from the opposing radar site are rotated through nearby bearings at the same range. Similarly, the rms difference values have a clear minimum in the baseline direction. In general, all the baseline comparisons exhibit this behavior to a greater extent than was seen in the mooring comparisons, which adds confidence to the bearing error estimates derived from the baseline comparisons.

The measured rms difference values range from 9.8 to 13.0 cm/s (Table I) for the expected baseline locations, which is a good indication of the intrinsic uncertainty in the radial current estimates. In terms of radial current error for an individual HF radar site, these values should be reduced by a factor of $\sqrt{2}$ leading to error estimates of 7–8 cm/s. Results involving the MLNG radar site are not detectably different than the other baseline pairs even though the MLNG HF radar operated near 25 MHz and the other sites operated near 13 MHz. Other studies have attempted to utilize frequency variations in this range to change the effective measurement depth and to look for evidence of velocity shear in the upper 2 m of the water column [25], [26]. If present, these results suggest that the shear in this case is not detectable beyond the measurement uncertainty.

It should be noted that the baseline results have been presented only for the data obtained using measured antenna patterns. Baseline results based on data obtained using ideal antenna patterns are generally worse (Table I). The performances of the two data sets are shown in terms of scatter plots in Fig. 10 for the expected baseline directions. Of the four baseline pairs, the SCRZ-to-NPGS pair exhibits the most significant improvement using measured antenna patterns instead of ideal antenna patterns, which is consistent with the dramatic improvement seen for the NPGS site when compared with radial current observations at the M1 mooring.

C. Drifter-Based Velocity Comparisons

The third type of radial validation information available in this paper is the comparison with drifter-derived radial currents in the directions of the various HF radar sites. To facilitate these comparisons, the GPS drifter positions (Fig. 1) were used to pro-

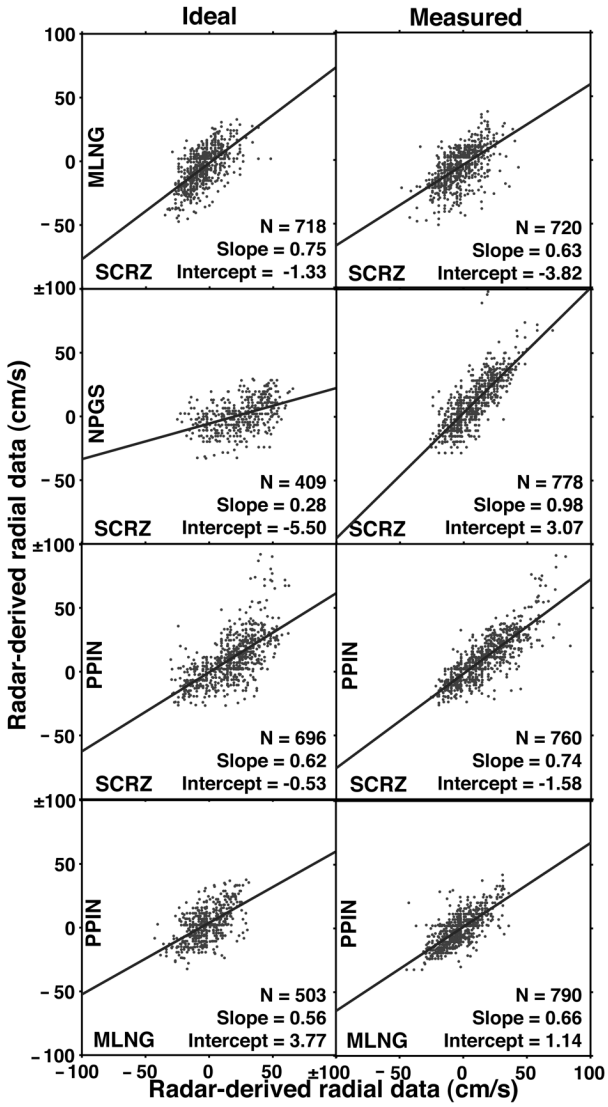

Fig. 10. HF radar-derived radial currents at the center point of overwater baseline pairs using ideal and measured antenna patterns. The number of hourly observations (N) and the slope and intercept for the best-fit linear prediction are also shown.

duce hourly velocity estimates and each vector velocity was projected into the direction of each of the four radar sites. As mentioned previously, the depth and spatial averaging characteristics of the drifter- and radar-derived radial currents are not directly matched. However, the distributed locations of the drifter observations with respect to bearing relative to the HF radar sites provides a unique opportunity to assess pointing errors across a wide range of angles. Assuming that bearing errors are independent of range, the drifter-radar observation pairs can be binned and analyzed as a function of bearing.

The drifter observation locations relative to 5° bearing bins are shown in Fig. 11 for each of the four radar sites; the correlation coefficients and rms differences as a function of bearing angle are shown in Fig. 12. The performance of the HF radar systems varies between sites and, in some cases, the performance varies dramatically for different bearing angles at the same site. At the SCRZ site, the rms radial current differences compared with drifter observations were larger for angles to the south of the radar site, including the directions to the PPIN and NPGS radar sites. For those angles between $-58°$ (302°) and $-83°$ (277°), which includes the angles with relatively large rms differences, the use of measured antennas patterns greatly improves the radar-to-drifter comparison results. For other angles between $-28°$ (332°) and $-58°$, there is very little difference between the results obtained using measured antenna patterns and those obtained using ideal antenna patterns. This is consistent with the pattern distortions shown in Fig. 4 for which ideal and measured antenna patterns diverge for angles less than about 300°. The correlation values between SCRZ and drifter observations show less variation with angle and antenna-pattern corrections than do the rms difference values. There is a sharp drop in correlation, however, at $-68°$ where the rms difference values are largest. In no case does the variation with angle appear correlated with the number of drifter versus radar observation pairs, which further suggests that the observed angular variations are, at least, partly related to systematic errors in bearing detection.

For the MLNG site, both the correlation and rms difference values are relatively constant as a function of angle. In addition, there is very little difference in the results based on measured or ideal antenna patterns, except for the correlation values at both extreme angles, which exhibit the anomalous characteristic of reduced correlation for results based on measured antenna patterns as compared with results based on ideal antenna patterns. The general lack of sensitivity to angle for the MLNG site is consistent with the results in Fig. 4 showing that site to have the least amount of observed antenna-pattern distortion.

Radial current data from the NPGS site exhibited the greatest difference between results obtained using measured or ideal antenna patterns when compared with observations at the M1 mooring or with other radar-derived baseline values. The drifter results as a function of angle in Fig. 12 and the summary statistics for the point-to-point matches in Fig. 13 are consistent with those findings. Correlation and rms difference values are dramatically altered and improved shifting from estimates obtained using ideal antenna patterns to those obtained using measured antenna patterns. Angular variations of the correlation and rms difference values, although still present, are also reduced for the estimates obtained using measured antenna patterns.

The final radar site at PPIN performed well compared with the drifter-derived radial velocity observations. There is some evidence of increased error for angles to the northwest. Unfortunately, the distribution of drifter observations did not adequately cover the wide range of viewing angles measured by the HF radar at PPIN (Fig. 11). The antenna-pattern observations in Fig. 4 suggest that larger errors should be expected for angles to the northwest and west, particularly for results obtained assuming ideal antenna patterns.

IV. Discussion

This paper has focused on the validation of remotely sensed ocean surface currents from SeaSonde-type HF radar systems. Hourly observations during the period July 22, 2003 through September 9, 2003 were used from four separate radar sites deployed around the shores of Monterey Bay, CA. Radial current

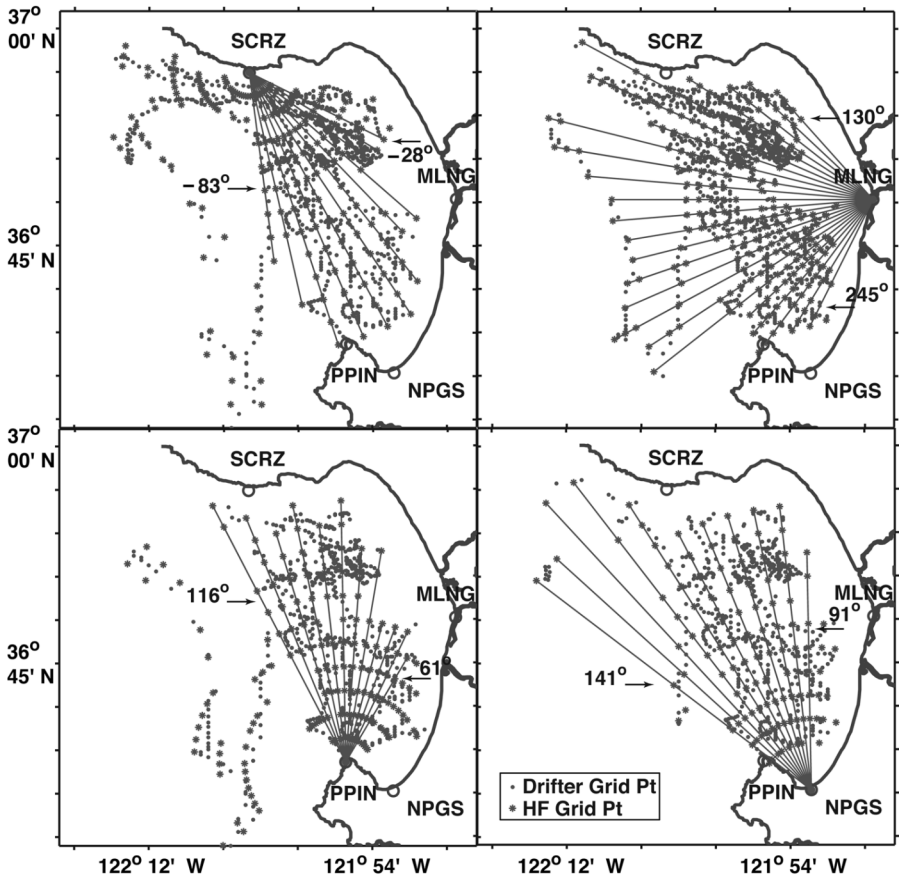

Fig. 11. Radial current observation locations (larger symbols) for which nearby drifter-derived radial current observations (smaller symbols) were available. The radial lines indicate the look directions over which comparison statistics were produced using radar- and drifter-derived radial velocities without regard to range.

estimates from each site were available based on both ideal and measured antenna patterns and those data sets were compared with radial velocity components from a moored ADCP and from 16 surface drifter trajectories. In addition, coverage overlaps between the four radar sites provided for a total of four overwater baselines on which radar-to-radar comparisons were made.

A summary of the validation results is given in Table I, which presents the temporal correlation coefficients and rms differences using the radar grid analysis cell geographically closest to the mooring location, drifter observation, or baseline center. Overall, the comparisons with the moored velocity observations exhibited larger rms differences and lower correlation coefficients than the comparisons with drifter observations or baseline estimates. The mooring observations used in this paper responded to ocean currents that were significantly deeper than those measured by the HF radar systems. In this sense, it is understandable that the mooring data returned less favorable comparisons. Particularly for hourly velocity data, it is well known that a significant amount of wind-driven energy that is present at the 1-m depth of the radar measurements is absent below 12 m where the ADCP observations in this paper began [22]. The drifter observations used in this paper responded to currents between the surface and 8 m. Results suggest a much closer relationship between the radar- and drifter-derived velocities than was seen for the mooring velocities.

In all cases, comparisons based on HF radar estimates obtained using measured antenna patterns were either much better than those obtained using ideal antenna patterns or were only slightly changed. These results can be added to the few prior studies in which improvements were documented using measured antenna patterns with SeaSonde-type HF radar systems (e.g., [8]). It should be stressed to all users and potential users of HF radar systems that the *in situ* receive antenna response as a function of angle must be measured and utilized for every installation. This is particularly true for direction-finding systems that are subject to bearing errors, but the in-place antenna patterns for larger, phased-array systems should also be measured to assess and avoid errors in the determination of radial velocity.

Focusing on results obtained using measured antenna patterns from either drifter or baseline comparisons, the rms differences obtained in this paper range from 9.8 to 13.0 cm/s. This suggests error estimates in the range of 6.9–9.2 cm/s for the HF radar-derived radial currents. It must be reiterated, however, that this error or uncertainty range is valid only if care is taken to use measured antenna patterns and to account for variations in measurement depths.

In addition to the clear benefits of using measured antenna patterns with SeaSonde-type HF radar systems, this paper provides evidence of substantial (up to 15°) residual bearing errors even when those measured antenna patterns are used. It is also clear that bearing errors for a given HF radar site are not

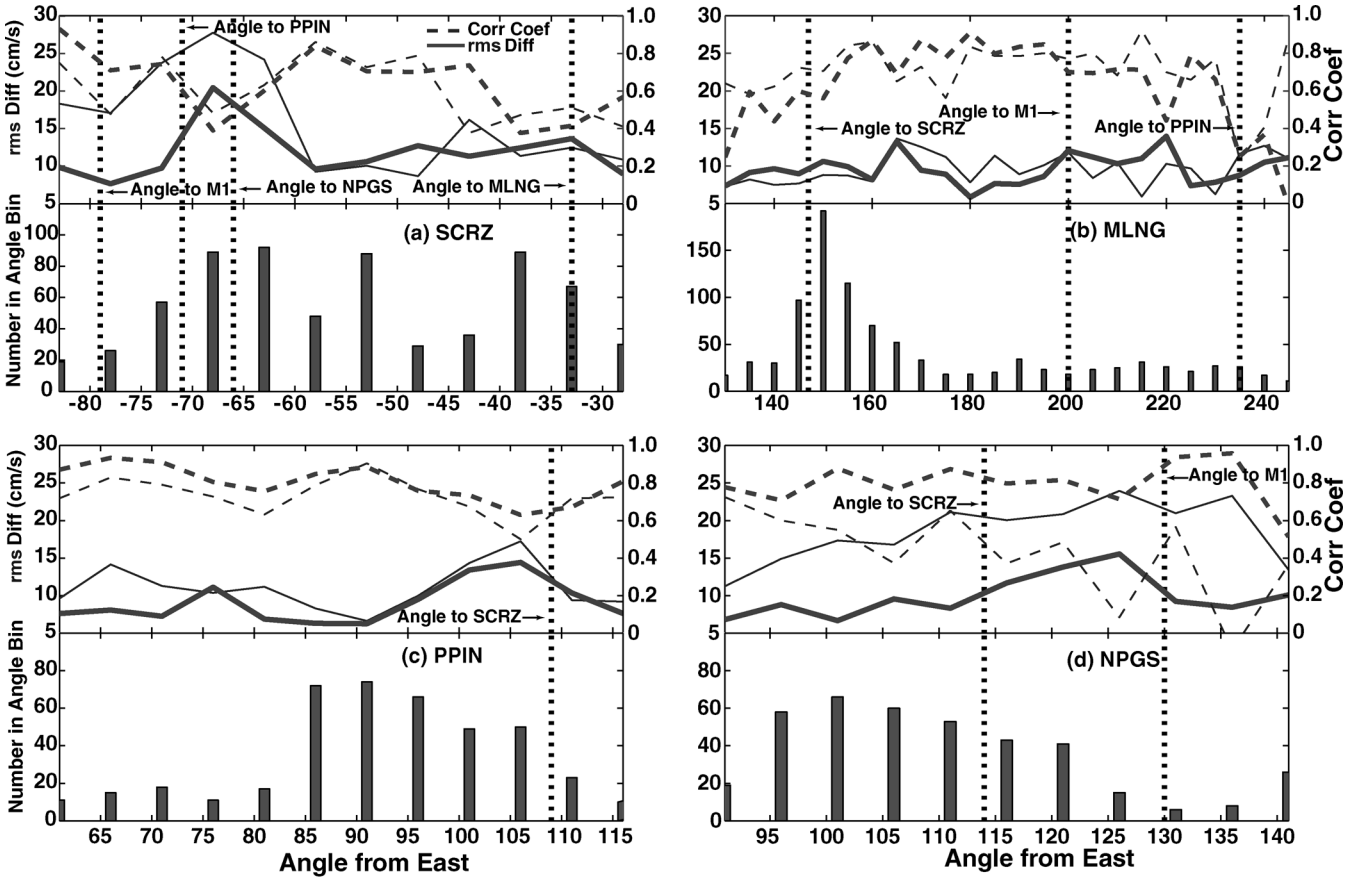

Fig. 12. Correlation coefficients (dashed) and rms difference values (solid) for radar-derived and drifter-derived radial currents in 5° angle bins with the number of hourly radial current pairs per bin (lower panels) for (a) SCRZ, (b) MLNG, (c) PPIN, and (d) NPGS. Results are shown for radar-derived radial currents based on ideal (thin) and measured (heavy) antenna patterns.

a constant with angle. That is, the errors cannot be corrected through a uniform rotation of the radial velocity data (unless, of course, a physical antenna alignment error is uncovered). The interaction of antenna-pattern distortions and the MUSIC direction-finding algorithm are complex and poorly documented. It can be seen from the several antenna-pattern measurements in Fig. 4 that distortions compared with the expected sinusoidal patterns can be severe. What is the limit of acceptable distortion? The answer is likely to depend on the shape of the distorted patterns, the multivalued nature of the radial current patterns, the horizontal distribution of wave energy, and the electromagnetic noise level, among other things. The observed patterns shown in Fig. 4 were averaged over 5° increments. The measured patterns without averaging exhibit rapid variations in some sectors. What is the appropriate amount of angular smoothing and what is the impact of smoothing with respect to the MUSIC algorithm?

Additional studies of the type conducted here may provide some answers to these questions, particularly studies with multiple shallow drifters covering a wide range of bearing angles. However, it is our contention that direct *in situ* validation studies will never adequately constrain the many factors effecting bearing detection using a fixed number of distorted antenna elements. It is essential that simulation studies of the type begun by [27] be conducted over a range of velocity, wave, and noise conditions and using a wide range of distorted antenna-pattern weighting functions. Only in simulations can the many factors effecting the performance of direction-finding algorithms be controlled and assessed. Laws *et al.* [27] investigated the effect of complex radial current patterns and signal-to-noise ratios on a particular implementation of MUSIC applied to an eight-element linear array HF radar system known as the multifrequency coastal radar (MCR). They stopped short, however, of assessing the performance of their MUSIC implementation in the presence of antenna element distortions; neither did they attempt to simulate the performance of the compact three-element SeaSonde system. Barrick and Lipa [28] report on simulations using the SeaSonde configuration, but their simulations involved only situations with ideal (i.e., perfect) antenna patterns. These early simulation studies must be expanded with the goal of better documenting the errors related to antenna-pattern distortions, including the possibility that some field sites should be considered "unusable" based on the observed antenna-pattern distortions.

Finally, we point to the optimistic result that antenna-pattern distortions remained relatively constant over periods exceeding one year based on the three HF radar sites for which we have repeated observations. This means that once we understand the optimal ways to use antenna-pattern measurements it is reasonable to expect those patterns to remain unchanged for long periods in the absence of major structural changes near the radar site.

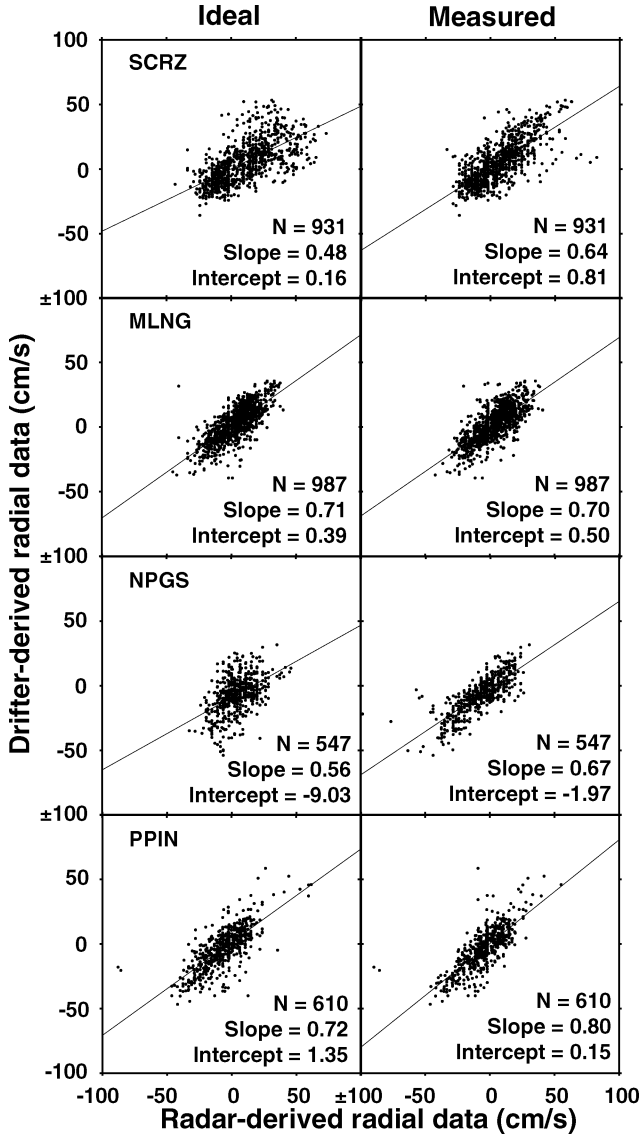

Fig. 13. HF radar- versus drifter-derived radial currents using ideal and measured antenna patterns. The number of hourly observations (N) and the slope and intercept for the best-fit linear prediction are also shown.

APPENDIX
BEARING DETERMINATION AND DIRECTION-FINDING SYSTEMS

Direction-finding HF radar systems, such as the SeaSonde, are particularly vulnerable to pointing errors. This is because direction-finding techniques, by definition, do not attempt to exploit real-aperture pointing methods in which receive antenna elements are separated by a sufficient number of wavelengths such that time delays in the receipt of information from one element to another can be used to determine the direction-of-arrival of the backscattered signals. Instead, direction-finding techniques rely upon the comparison of information received by different antenna elements located at, effectively, the same location. Direction-finding systems can still utilize small physical separations and phase differences between antenna elements, such as in the configuration for the earliest CODAR-type instruments [29], [11], or they can rely more heavily on amplitude differences measured by the colocated antenna elements to determine bearing, as is the case for the SeaSonde systems studied in this paper.

In terms of data processing techniques, real-aperture or beamforming systems differ fundamentally from direction-finding systems in that the former make use of the antenna element separations up front to create individual Doppler backscatter spectra for every bearing angle at a given range. By contrast, direction-finding systems are forced to work with a single Doppler spectrum that contains the convolved information from all bearing angles at a given range. In addition to its relative simplicity, the beamforming technique has the advantage of producing individual spectra whose second-order contributions can be more directly analyzed for surface wave conditions (e.g., [30]). However, direction-finding systems also have distinct advantages, such as their more practical size and the fact that observations from a single site are not limited to just 90° of viewing angle, which is the case for beamforming systems. Direction-finding systems can return data from a full 360° from locations such as offshore platforms. In this paper, for example, data covering nearly 270° was obtained from the PPIN HF radar site.

This paper is focused on the performance of the SeaSonde direction-finding HF radar systems, which utilize measurements from three antenna elements. Example Doppler spectra from the SCRZ radar site are shown in Fig. 14. The broadened region of Bragg-resonant or first-order returns in the figure should be compared with the narrow peaks in Doppler spectra returned by long phase-array systems (e.g., [10]). Physically, the antenna components consist of two orthogonally mounted loop elements and one monopole element. It should be made clear that all systems of this type depend fundamentally on knowing and correctly applying the angular response functions of the colocated antenna elements. Antenna-pattern errors translate into bearing errors in direct but complicated ways. The degrees of freedom in this type of measurement system are associated with the number of antenna elements and the particular inversion algorithm used to extract bearings. Bearing uncertainties are also influenced by the ocean wave conditions and the spatial complexity of the ocean current patterns. The inversion algorithms themselves have evolved in recent years; many systems, including the SeaSonde, now use some form of MUSIC [31], [24], which differs substantially from earlier alternatives that were based more directly on the arctangent of amplitude ratios or time delays [32], [11]. MUSIC is a statistical method that, in principle, can return the direction-of-arrival of $N-1$ signals for a given Doppler frequency (i.e., radial current speed), where N is the number of antenna elements. In the case of the SeaSonde, N is 3 and, therefore, either one or two bearing solutions exist. However, because both approaching and receding portions of a given spectrum are processed independently, up to four different bearing solutions can be assigned to a given radial velocity. Although MUSIC is a statistical algorithm, the critical direction information is still contained in the ratio of amplitudes and phases of the two loop antenna elements normalized by the omnidirectional monopole element, which is why those functions are plotted in Fig. 4.

Finally, bearing errors and radial current errors in general for SeaSonde-type direction-finding systems are influenced by the

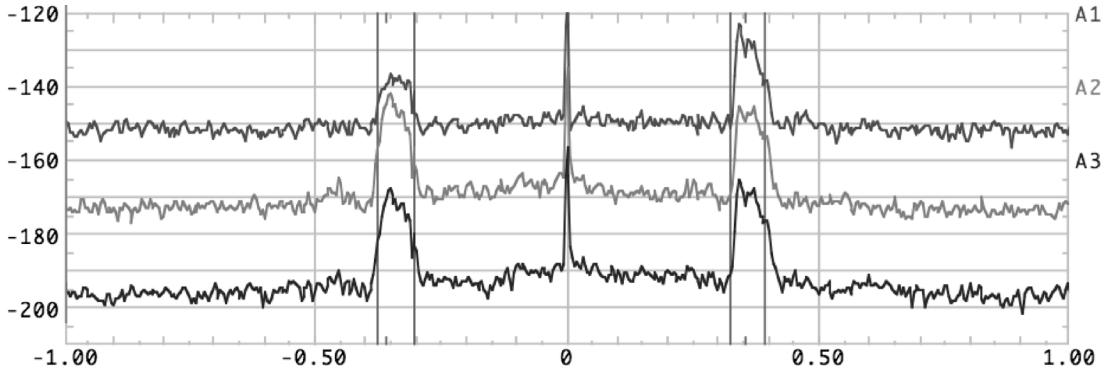

Fig. 14. Sample Doppler spectra, offset by 20 dB, from range cell 15 (approximately 45 km offshore) for loop-1 (upper), loop-2 (middle), and monopole (lower) antenna elements for the SeaSonde HF radar system at SCRZ at 18:00:00Z, on August 7, 2005. Axes labels show power level in dB and Doppler frequency in Hz above or below the 12.17-MHz operating frequency. Individual Doppler bins within the designated approaching (positive) and receding (negative) Bragg regions would be processed to determine direction-of-arrival (bearing) using the relative measurements from the three antenna elements.

spectral resolution, which is determined by $v_{\rm res} = \lambda_r/2n_{\rm seg}\Delta t$, where λ_r is the radar wavelength, $n_{\rm seg}$ is number of samples, and Δt is the pulse repetition period or sampling rate [27]. For the SeaSonde units in Monterey Bay, the velocity resolution is between 2.3 and 4.6 cm/s, depending on the operating frequency.

ACKNOWLEDGMENT

The authors would like to thank G. Friederich of MBARI and F. Bahr of the Naval Postgraduate School for assistance with the drifter and moored observations, respectively, and S. Ramp for helpful comments. K. C. Kim would like to thank the international student program at the Naval Postgraduate School.

REFERENCES

[1] J. D. Paduan, P.-M. Kosro, and S. M. Glenn, "A national coastal ocean surface current mapping system for the United States," *Marine Tech. Soc.*, vol. 38, pp. 102–108, 2004.

[2] K.-W. Gurgel, G. Antonischki, H.-H. Essen, and T. Schlick, "Wellen radar WERA, A new ground-wave based HF radar for ocean remote sensing," *Coastal Eng.*, vol. 37, pp. 487–511, 1999.

[3] R. D. Chapman and H. C. Graber, "Validation of HF radar measurements," *Oceanography*, vol. 10, no. 2, pp. 76–79, 1997.

[4] J. D. Paduan and L. K. Rosenfeld, "Remotely sensed surface currents in Monterey Bay from shore-based HF radar (CODAR)," *J. Geophys. Res.*, vol. 101, pp. 20 669–20 686, 1996.

[5] H. C. Graber, B. K. Haus, L. K. Shay, and R. D. Chapman, "HF radar comparisons with moored estimates of current speed and direction: Expected differences and implications," *J. Geophys. Res.*, vol. 102, pp. 18 749–18 766, 1997.

[6] L. K. Shay, S. J. Lentz, H. C. Graber, and B. K. Haus, "Current structure variation detected by high frequency radar and vector measuring current meters," *J. Atmos. Ocean. Technol.*, vol. 15, pp. 237–256, 1998.

[7] B. M. Emery, L. Washburn, and J. A. Harlan, "Evaluating radial current measurements from CODAR high-frequency radars with moored current meters," *J. Atmos. Ocean. Technol.*, vol. 21, pp. 1259–1271, 2004.

[8] J. D. Paduan, D. Barrick, D. Fernandez, Z. Hallock, and C. Teague, "Improving the accuracy of coastal HF radar current mapping," *Hydro Int.*, vol. 5, pp. 26–29, 2001.

[9] J. Kohut, S. Glenn, and D. E. Barrick, "SeaSonde is integral to coastal flow model development," *Hydro Int.*, vol. 3, no. 3, pp. 32–35, 1999.

[10] J. D. Paduan and H. C. Graber, "Introduction to high frequency radar: Reality and myth," *Oceanography*, vol. 10, pp. 36–39, 1997.

[11] K.-W. Gurgel, "Shipborne measurement of surface current fields by HF radar," *Onde Electr.*, vol. 74, pp. 54–59, 1994.

[12] R. H. Stewart and J. W. Joy, "HF radio measurements of surface currents," *Deep-Sea Res.*, vol. 21, pp. 1039–1049, 1974.

[13] H.-H. Essen, E. Mittelstaedt, and F. Schirmer, "On near-shore surface current measurements by means of radar," *Deutsche Hydrographische Zeitschrift*, vol. 34, pp. 1–14, 1981.

[14] K. Laws, "Measurements of near surface ocean currents using HF radar," Ph.D. dissertation, Physics Dept., Univ. California Santa Cruz, Santa Cruz, CA, 2001.

[15] K. Laws, J. D. Paduan, and D. M. Fernandez, "Effect of Stokes drift on HF radar measurements," in *Proc. 1st Int. Workshop Radiowave Oceanogr.*, 2003, pp. 49–55.

[16] K. C. Kim, "Calibration and validation of high-frequency radar ocean surface current mapping," M.S. thesis, Oceanography Dept., Naval Postgraduate School, Monterey, CA, 2004.

[17] D. C. Melton, "Remote sensing and validation of surface currents from HF radar," M.S. thesis, Oceanography Dept., Naval Postgraduate School, Monterey, CA, 1995.

[18] B. Lipa, J. A. Rizoli, Ed., "Uncertainties in SeaSonde current velocities," in *Proc. IEEE/OES 7th Working Conf. Current Meas. Technol.*, New York, NY, Mar. 2003, pp. 95–100.

[19] J. T. Kohut and S. M. Glenn, "Improving HF radar surface current measurements with measured antenna beam patterns," *J. Atmos. Ocean. Technol.*, vol. 20, pp. 1303–1316, 2003.

[20] F. P. Chavez, J. T. Pennington, R. Herlien, H. Jannasch, G. Thurmond, and G. E. Friederich, "Moorings and drifters for real-time interdisciplinary oceanography," *J. Atmos. Ocean. Technol.*, vol. 14, pp. 1199–1211, 1997.

[21] M. H. Pickett and J. D. Paduan, "Ekman transport and pumping in the California current based on the U.S. Navy's high-resolution atmospheric model (COAMPS)," *J. Geophys. Res.*, vol. 108, no. C10, p. 3327, 2003.

[22] J. D. Paduan and M. S. Cook, "Mapping surface currents in Monterey Bay with CODAR-type HF radar," *Oceanography*, vol. 10, pp. 49–52, 1997.

[23] E. T. Petruncio, L. K. Rosenfeld, and J. D. Paduan, "Observations of the internal tide in Monterey Submarine Canyon," *J. Phys. Oceanogr.*, vol. 28, pp. 1873–1903, 1998.

[24] D. E. Barrick and B. J. Lipa, "Evolution of bearing determination in HF current mapping radars," *Oceanography*, vol. 10, pp. 72–75, 1997.

[25] C. C. Teague, J. F. Vesecky, and Z. R. Hallock, "A comparison of multifrequency HF radar and ADCP measurements of near-surface currents during COPE-3," *IEEE J. Ocean. Eng.*, vol. 26, no. 3, pp. 399–405, Jul. 2001.

[26] L. A. Meadows, "High frequency radar measurements of friction velocity in the marine boundary layer," Ph.D. dissertation, Ocean Sciences Dept., Univ. Michigan, Ann Arbor, MI, 2002.

[27] K. Laws, D. M. Fernandez, and J. D. Paduan, "Simulation-based evaluations of HF radar ocean current algorithms," *IEEE J. Ocean. Eng.*, vol. 25, no. 4, pp. 481–491, Oct. 2000.

[28] D. E. Barrick and B. J. Lipa, "Comparison of direction-finding and beam-forming in HF radar ocean surface current mapping," National Oceanic and Atmospheric Administration, Rockville, MD, Phase 1 SBIR Final Rep., 1996, Contract No. 50-DKNA-5-00092.

[29] D. E. Barrick, M. W. Evans, and B. L. Weber, "Ocean surface currents mapped by radar," *Science*, vol. 198, pp. 138–144, 1977.
[30] L. T. Wyatt, "HF radar for real-time current, wave and wind monitoring," *Hydro Int.*, vol. 9, no. 3, pp. 30–31, 2005.
[31] R. O. Schmidt, "Multiple emitter location and signal parameter estimation," *IEEE Trans. Antennas Propag.*, vol. Ap-34, no. 3, pp. 276–280, Mar. 1986.
[32] B. J. Lipa and D. E. Barrick, "Least-squares method for the extraction of surface currents from CODAR crossed-loop data: Application at ARSLOE," *IEEE J. Ocean. Eng.*, vol. 8, no. 4, pp. 226–253, Oct. 1983.

Jeffrey D. Paduan received the B.S.E. degree in engineering science from the University of Michigan, Ann Arbor, in 1982 and the Ph.D. degree in physical oceanography from Oregon State University, Corvallis, in 1987. His general field of study has been ocean current patterns from satellite-tracked drifting buoys and high-frequency radar installations.

He has worked as a Research Technician at Great Lakes Environmental Research Laboratory, NOAA and as a Post-Doctoral Fellow at the Scripps Institution of Oceanography, University of California at San Diego, La Jolla. He is now an Associate Professor of Oceanography at the Naval Postgraduate School, Monterey, CA, where he has been on the faculty since 1991. In 1997, he coedited a special issue of the Oceanography Society's journal (*Oceanography*, vol. 10, no. 2) devoted to high-frequency radar applications. In 2001, he cofounded the International Radiowave Oceanography Workshop (ROW; http://radiowaveoceanogrphy.org), which continues to be an important focal point for this growing branch of marine science.

Dr. Paduan is a member of the American Geophysical Union, the Oceanography Society, and the American Meteorological Society (AMS). He has served on the AMS committee for Meteorology and Oceanography of the Coastal Zone, on the steering committee for the Ocean.US community workshop on ocean observing systems, and, recently, as Chair of the Ocean.US steering committee for the national surface current mapping initiative. Currently, he is a member of the Monterey Bay National Marine Sanctuary's integrated monitoring network science steering committee and of the state-wide science advisory panel for the Marine Life Protected Act initiative. In addition, he is now serving as President of the governing council for the regional association known as the Central and Northern California Ocean Observing System. In March 1999, he overviewed the high-frequency radar applications research area as the keynote speaker for the IEEE 6th Working Conference on Current Measurement Technology.

Kyung Cheol Kim received the B.S. degree in physical oceanography from the Republic of Korea (ROK) Naval Academy, Korea, and was commissioned an Ensign in 1993 and the M.S. degree in physical oceanography from the Naval Postgraduate School. Monterey, CA, in 2004.

He is a Lieutenant Commander in the Korean Navy. During his service career, he received basic and primary surface warfare officer training at the Naval Education and Training Command in Chinhae, Korea and at the ROK Naval War College in Taejon, Korea, respectively. He received further training at the International Surface Warfare School in San Diego, CA, in 1997. After service at ROK Fleet Command, he served as Operations Liaison officer with the U.S. Naval Forces in Korea, from 2000 to 2002, during which he received the Navy and Marine Corps Commendation Medal for meritorious service. At present, he is serving as the Operations Officer onboard ROKS Cheonghaejin (ASR-21).

Michael S. Cook received the B.S. degree in environmental science from Wilkes University, Wilkes-Barre, PA, in 1984, and the M.S. degree in oceanography from Texas A & M University, College Station, in 1990.

Previously, he has worked as an Environmental Technician monitoring acid mine drainage and urban storm water pollutant levels, an Environmental Consultant, and a Manager of a water quality analysis laboratory. He is currently an Oceanographer at the Naval Postgraduate School, Monterey, CA, where he has been analyzing coastal velocity observations for the effects of winds and tides and working to develop an open-source software package tailored to high-frequency radar applications.

Francisco P. Chavez received the Ph.D. degree in botany from Duke University, Durham, NC, in 1987.

He is a Senior Scientist at the Monterey Bay Aquarium Research Institute (MBARI), Moss Landing, CA. His research interests are in long-term ocean observing and the biology and chemistry of the oceans in relation to global change.